Efferent control of hearing sensitivity and protection via inner ear supporting cells

Hong-Bo Zhao, Li-Man Liu, Ling Mei, Ning Yu, Jin Chen, Yan Zhu, Chun Liang

Dept. of Otolaryngology, University of Kentucky Medical Center, Lexington, KY 40536

Running title: A new efferent control pathway for hearing sensitivity

Corresponding Author:

Hong-Bo Zhao, Ph.D./M.D.
Professor
Dept. of Otolaryngology
University of Kentucky Medical Center
800 Rose Street
Lexington, KY 40536 – 0293
USA

Tel: 859-218-2138
Fax: 859-257-5096
E-mail: hzhao2@uky.edu

Keywords: Cochlear efferent system, MOC, ACh, gap junction, Cx26, supporting cells, outer hair cell electromotility, active cochlear amplification, knockout, hearing, noise.

Summary

It is critical for hearing that the descending cochlear efferent system provide negative feedback to hair cells to regulate hearing sensitivity and provide protection from noise. The medial olivocochlear (MOC) efferent nerves project to outer hair cells (OHCs) and inhibit OHC electromotility, which is an active cochlear amplification and can increase hearing sensitivity. Here, we report that the MOC efferent nerves also have functional innervation with the cochlear supporting cells to regulate hearing sensitivity. The MOC efferent nerve fibers and the corresponding MOC neurotransmitter acetylcholine (ACh) receptors were visible in the cochlear supporting cells. Application of ACh in the cochlear supporting cells could also evoke inward currents in a dose-dependent manner and reduced gap junctional (GJ) coupling between the cochlear supporting cells, which consequently declined electromotility in OHCs. This indirect inhibitory effect through the mediated GJs between the cochlear supporting cells on OHC electromotility was consistent and enhanced the direct inhibition of ACh on OHC electromotility but had long-lasting influence. In vivo experiments further demonstrated that deficiency of this GJ-mediated efferent control pathway declined the regulation of active cochlear amplification and impaired the protection from noise trauma. Our findings reveal a new pathway for the cochlear efferent system to control hearing sensitivity, and also demonstrate that this supporting cell GJ-mediated efferent pathway is critical for control of hearing sensitivity and the protection of hearing from noise trauma.

Significance statement

The cochlear efferent system provides a negative feedback loop to hair cells and plays a critical role in the regulation of hearing sensitivity and protection from noise trauma. In this study, we found that besides projection to outer hair cells (OHCs), the medial olivocochlear (MOC) efferent system has innervation with cochlear supporting cells and regulate gap junctions (GJs) between supporting cells to control OHC electromotility and hearing sensitivity. Deficiency of this supporting cell GJ-mediated efferent pathway could impair the regulation of active cochlear amplification and increased susceptibility to noise. Our findings demonstrate that the MOC efferent system not only directly inhibits OHC activity but also can control GJs between supporting cells to regulate hearing sensitivity, which plays a critical role in the protection from noise trauma.

Introduction

The cochlea is the auditory sensory organ in mammals. In addition to ascending auditory nerves projecting to the brain, the cochlea also receives descending efferent fibers to hair cells forming a negative feedback loop to regulate hair cell activity, which plays an important role in the regulation of hearing sensitivity, the discrimination of sounds in background noise, and protection from acoustic trauma (Guinan, 2006; Lustig, 2006; Clause et al., 2017; Boero et al., 2018). The cochlear efferent fibers are composed of the medial olivocochlear (MOC) nerves and lateral olivocochlear (LOC) nerves. The MOC nerves originate from the medial superior olivary nucleus in the brainstem projecting to outer hair cells (OHCs) in the cochlea, whereas the LOC nerves project from the lateral superior olivary nucleus in the brainstem to inner hair cells (IHCs) and form synapses with the dendrites of type I afferent auditory nerves under the IHCs. The MOC fibers are cholinergic fibers and acetylcholine (ACh) is a primary neurotransmitter, and the LOC has cholinergic fibers and dopaminergic fibers, releasing ACh, dopamine, and other neurotransmitters (Eybalin, 1993; Lustig, 2006; Maison et al., 2012).

The cochlea also has supporting cells to support hair cell function. For example, Deiters cells (DCs) and pillar cells (PCs) in vicinity of OHCs act as a scaffold to support OHCs standing on the basilar membrane allowing OHC motility amplifying sound induced basilar membrane vibration (Brownell et al., 1985; Ashmore, 2008). This active cochlear amplification is critical for hearing. Deficiency of the active cochlear amplification can induce hearing loss (Zheng et al., 2000; Liberman et al., 2002; Ashmore, 2008). In anatomy, the cochlear supporting cells are extensively coupled by

gap junctions (GJs) (Kikuchi et al., 1995; Forge et al., 2003; Zhao and Yu, 2006). Cx26 and Cx30 are the predominant GJ isoforms in the cochlea (Forge et al., 2003; Zhao and Yu, 2006; Liu and Zhao, 2008). However, there is neither GJ nor connexin expression in the hair cells or between hair cells and supporting cells (Kikuchi et al., 1995; Zhao and Santos-Sacchi, 1999; Zhao and Yu, 2006; Yu and Zhao, 2009). Recently, increasing evidence demonstrated that supporting cells in the cochlea have more than simple "supporting" functions, such as participating in active cochlear amplification (Zhu et al., 2013, Zong et al., 2017). Most importantly, Cx26 mutations can cause nonsyndromic hearing loss and are responsible for >50% of cases of nonsyndromic hearing loss (Castillo and Castillo, 2011; Chan and Chang, 2014; Wingard and Zhao, 2015). This further indicates that the cochlear supporting cells play critical role in hearing. However, the function of the supporting cells in the cochlea still remains largely unexplored.

It is critical for hearing that the cochlear efferent system provides a negative feedback to hair cells to regulate hearing sensitivity and protect against acoustic trauma. Prior studies demonstrated that the cochlear efferent nerves directly project to hair cells and their associated afferent auditory nerves to inhibit hair cell and auditory nerve activities (Guinan, 2006; Lustig, 2006). In this report, we found that the MOC efferent nerves also innervate supporting cells and regulate GJs between the supporting cells to control OHC electromotility and hearing sensitivity. Deficiency of this supporting cell GJ-mediated efferent control pathway declined the regulation of active cochlear amplification and increased susceptibility to noise.

Results

Innervation of MOC nerves in the cochlear supporting cells

It is well-known that the MOC nerves project to OHCs in the cochlea. Fig. 1 shows that the MOC fibers, which were labeled by neurofilament (NF), passed through the cochlear tunnel projecting to OHCs. However, in addition to projection to the OHCs, MOC fibers also had innervations in the cochlear supporting cells (Fig. 1B&C). In the cross-cochlear view of 3D confocal images (Fig. 1D&E), it is clearly visible that MOC nerves had branches projecting to DCs, PCs, and Hensen cells (HCs). The neural branch also could project from the first row of OHCs to the second and third row of DCs (indicated by a white arrowhead in Fig. 1D). The MOC nerve is an acetylcholinergic fiber. Immunofluorescent staining for ACh receptors (AChR) shows that besides intensive labeling at the OHC basal pole, AChR labeling is visible at the cochlear supporting cells with MOC nerves (Fig. 1F&G). These data demonstrated that there are innervations of MOC nerves in the cochlear supporting cells, in particular, in DCs.

Fig. 1

Responses of the cochlear supporting cells to MOC neurotransmitter ACh

We further tested whether supporting cells have response to MOC neurotransmitter. ACh is a MOC neurotransmitter. Fig. 2 shows that application of ACh in the DC could evoke a typical inward current as seen in the OHC (Fig. S3B). ACh-elicited current in the supporting cells had a fast inward phase and then decayed (Fig. 2B and Fig. S1A). The ACh-evoked inward current is reversible and repeatable (Fig. S1B). As ACh was

repeatedly applied, the inward current could be recordable repeatedly. In addition, the ACh-evoked current in the group of supporting cells was larger than that recorded in the single cells because of GJ-coupling between cells (Fig. S1C&D). To further evaluate the responses to ACh, we measured dose-curve of ACh-evoked current in the single DC (Fig. 2E). The middle concentration of ACh (EC_{50}) was 91.8 μM and Hill's coefficient was 1.67.

Fig. 2

Effect of ACh on gap junctions between cochlear supporting cells

GJ is a major anatomic character in the cochlear supporting cells and has a critical function in hearing. We further assessed the effect of ACh on GJs between the cochlear supporting cells (Fig. 3). Since GJ channel is an intercellular channel and provides an electronic conduit between cells, GJ-coupling between the cochlear supporting cells can be assessed by input capacitance (C_{in}) measurement (Zhao and Santos-Sacchi, 1998; Zhu and Zhao, 2012). Fig. 3 shows that application of ACh could reduce C_{in}, i.e., uncoupling (reducing) GJs between cells. In Fig. 3A, C&D, C_{in} in pairs of cells was reduced to a half value after application of 0.5 mM ACh, indicating that two cells in a cell pair were uncoupled, i.e., GJ channels were closed. Fig. 3B also showed that C_{in} in a 3-HC group appeared a step-reduction, further demonstrated ACh-induced GJ-uncoupling in a cell group. The uncoupling effect of ACh was reversible (Fig. 3A&C). After stop of perfusion of ACh, C_{in} was increased and recovered to the coupled level. However, C_{in} had no apparent change in single cell for application of ACh, even ACh-evoked inward currents

were clearly visible in single cell (Fig. S2). This further demonstrated that the C_{in} measurement is not affected by membrane current changes.

Fig. 3

To further assess the effect of ACh on GJ function, we also used fluorescence recovery after photobleaching (FRAP) to directly measure GJ permeability (Fig. 4). The fluorescence in one cell in the outer supporting cell (DC and HC) area in the cochlear sensory epithelium was bleached by laser zapping (Fig. 4A). After bleaching, fluorescence in the bleached cell gradually recovered as fluorescent dye diffused back from neighboring cells through GJs (Fig. 4A&B). The speed of the FRAP is inversely propotional to GJ permeability. Fig. 4B&C shows that after application of 0.5 mM ACh, the recovery time constant of FRAP was increased to 69.3±5.69 s (Fig. 4C). In comparison with the time constant (45.8±4.68 s) in the control group without ACh treatment, ACh significantly increased the recovery time constant of FRAP more than 50% ($P<0.001$, one-way ANOVA with a Bonferroni correction). That is, ACh reduced GJ permeability between cochlear supporting cells. Moreover, the effect of ACh on GJ permeability appeared slowly development on the order of minutes (Fig. 4D). The time constant of the effect of ACh on GJ-permeability was around 11.0 min. Glutamate is thought to be the putative neurotransmitter of the synapses between OHCs and type II auditory nerves (Liberman, 1980; Matsubara et al., 1996). Fig. 4B&C show that application of glutamate (0.2 mM) had no significant effect on GJ permeability between

supporting cells. The recovery time constant was 42.8±4.65 s and had no significant difference from that in the control group (P=0.33, one-way ANOVA).

Fig. 4

Influence of changes in gap junctions between cochlear supporting cells on outer hair cell electromotility

As shown in Fig. 1A and Fig. 5A, OHCs constrained by DCs stand on the basilar membrane. Since OHC electromotility is tension (or load)-dependent (Iwasa, 1993; Kakahata and Santos-Sacchi, 1995; Ashmore 2008, Rabbitt, 2020), any changes in DCs could alter tension (or load) on OHCs to affect OHC electromotility even there is no direct GJ between DCs and OHCs (Yu and Zhao, 2009). Fig. 5 shows the effect of uncoupling of GJs between DCs on OHC electromotility. Since OHCs also have ACh receptors (Fig. 1G&F, and also see Elgoyhen et al., 1994; Gomez-Casati et al., 2005), this could interrupt the assessment of the effect of ACh-induced uncoupling of GJs between DCs on OHC electromotility. We used a GJ channel blocker octanol (10 mM) to uncouple GJs between DCs. Fig. 5B-D shows that application of 10 mM octanol uncoupled GJs between DCs (Fig. 5B) and caused large current changes by uncoupling (Fig. 5C). After uncoupling, C_{in} and current was reduced (Fig. 5B&C). This uncoupling induced OHC electromotility associated nonlinear capacitance (NLC) shifting to left side, i.e., to hyperpolarization negative voltage to reduce active cochlear amplification (Fig. 5D). Moreover, since uncoupling GJs between DCs could induce large current changes DCs, we did double patch clamp recording to simulate the effect of GJ uncoupling

induced current changes in DCs on OHC electromotility. OHC and DC in a pair of OHC and DCs were simultaneously recorded by double patch clamp (Fig. 5A). When changes in hold currents in the DCs to mimic the current changes in uncoupling of GJs, NLC in the OHC had significantly changes and shifted to left side (Fig. 5E) as the same as seen in the uncoupling of GJs between DCs (Fig. 5D).

Fig. 5

This left shifting in NLC is also consistent with the direct effect of ACh on OHC electromotility. Fig. S3 shows that application of ACh could evoke an inward current in the OHC and shifted NLC to left hyperpolarization direction. The shift is also reversible and repeatable. After stop of application of ACh, the peak voltage (V_{pk}) of NLC could returned to pre-application level (Fig. S3D).

Deficiency of the GJ-mediated control pathway impairs active cochlear amplification regulation and increases susceptibility to noise

To further assess the function of this GJ-mediated efferent control pathway in vivo, we targeted-deleted Cx26 expression in DCs to eliminate this control pathway. Fig. 6 shows that deletion of Cx26 in DCs decline the active cochlear amplification and regulation. Active cochlear amplification measured as distortion product otoacoustic emission (DPOAE) in Cx26 conditional knockout (cKO) mice was reduced (Fig. 6B&C). The gain of amplification, which was measured by DPOAE re f_1 amplitude, was also reduced (Fig. 6D). In Cx26 cKO mice, the gain regulation assessed by the I/O function

was also impaired (Fig. 6D). The gain in wild-type (WT) mice kept almost consistent and only had slight increase in lower sound level and then slightly decreased at the high-intensity, while the gain of DPOAE in Cx26 cKO mice was significantly reduced as the sound intensity increased (Fig. 6D). Thresholds of auditory brainstem response (ABR) in Cx26 cKO mice also showed moderate hearing loss, especially at the high frequency range (Fig. S4).

Fig. 6

We further tested the protective function of this supporting cell GJ-mediated efferent pathway. Fig. 7 shows that deficiency of this pathway could increase susceptibility to noise trauma. After exposure to ~96 dB wide noise for 2-hr, the WT mice had quickly a recovery in 3 days and completely recovered at post-exposure day 28 in DPOAE and ABR recordings (Fig. 7C&D). However, DPOAE in Cx26 cKO mice had no recovery in 3 day after exposure (Fig. 7A) and was continuously reduced to reach the maximum reduction at post-exposure day 3 (a blue arrow indicated in Fig. 7A) instead of post-exposure day 1 seen in the WT mice (Fig. 7C). Moreover, the reduction in DPOAE in Cx26 cKO mice was not recovered after noise exposure (Fig. 7A), while DPOAE in WT mice was quickly recovered in post-day 3 and completely recovered at post-exposure day 28 for the same noise-exposure (Fig. 7C). ABR threshold in Cx26 cKO mice also had larger increase after noise exposure and did not return to the control levels in control Cx26 cKO mice without noise exposure at the same age (Fig. 7B). As reported previously (Zong et al., 2017), it is noted that the control Cx26 cKO mice also had a progressive hearing loss and DPOAE was also slowly decreased with age increased (Fig. 7A&B).

Fig. 7

Discussion

In this experiment, we found that efferent MOC nerves have innervations in the cochlear supporting cells with ACh receptor expression (Fig. 1). Application of MOC neurotransmitter ACh could evoke inward current in the cochlear supporting cells and reduced GJs between them (Figs. 2-4), which eventually affected OHC electromotility (Fig. 5). Deficiency of this supporting cell GJ-mediated efferent control pathway could decline the regulation on active cochlear amplification and increased susceptibility to noise (Figs. 6-7). Taken together, these data demonstrate a new MOC efferent pathway and mechanism for control of OHC electromotility and hearing sensitivity and the protection from noise trauma (Fig. 8).

Fig. 8.

Our finding that MOC nerves has a branch projecting to the cochlear supporting cells (Fig. 1) is consistent with previous reports. It has been reported that there are nerve innervations in the cochlear supporting cells and form chemical synapses with outer supporting cells (DCs and HCs) (Wright and Preston, 1976; Stopp and Comis, 1979; Liberman et al., 1990; Nadol and Burgess, 1994; Burgess et al., 1997; Bruce et al., 2000). However, the source, function, and significance of these neural innervations are unclear or under debated (Fechner et al., 1998, 2001). In this study, we used multiple methods

and assessments demonstrating that MOC nerves have branches projecting to supporting cells and regulate GJ-coupling between them (Figs. 2-4), which could consequently influence OHC electromotility (Fig. 5). This effect on OHC electromotility is as the same as the direct effect of ACh on OHCs (Fig. S3), and could shift OHC electromotility to left hyperpolarization direction (Figs. 5 and S3). These data indicate that this supporting cell GJ-mediated pathway could enhance the direct inhibition of MOC efferent nerves on OHC function. In particular, since supporting cells are extensively coupled by GJs, any small changes could be amplified (Fig. S1). Thus, this efferent regulation via supporting cell GJs could play a critical role in the regulation of active cochlear amplification and protection from noise trauma. Indeed, impairment of this supporting cell GJ-mediated pathway led to significant damage in active cochlear amplification and protection from noise trauma (Figs. 6-7).

In addition, in comparison with direct effect of ACh on OHC electromotility which showed fast and quick (Fig. S3), the regulation via supporting cell GJs had long-lasting effect (Fig. 5). It is well-known that the MOC activity has a slow effect on the order of minutes in addition of the fast effect (Guinan, 2006). However, the underlying mechanism for this slow MOC effect is unclear. This supporting cell GJ-mediated control pathway may play an important role in the slow MOC effect. The slow MOC effect plays a critical role in noise protection. Indeed, deficiency of this pathway by targeted-deletion of Cx26 in the DCs led the long-term reduction in DPOAE; the DPOAE reduction and ABR threshold increase after noise exposure were not recovered (Fig. 7A&B). In comparison with WT mice, ABR threshold increase in Cx26 cKO mice was also larger

than that in WT mice for the same noise exposure (Fig. 7B&D). Moreover, the noise-induced reduction in DPOAE reached the maximum level at the post-exposure day 3 in Cx26 cKO mice (Fig. 7A) instead of day 1 seen in WT mice (Fig. 7C). These data demonstrated that this supporting cell GJ-mediated pathway plays a critical role in the slow MOC effect and protection from noise trauma.

It has been reported that supporting cells may also have innervations of the branches from the type II auditory nerve fibers under OHCs (Fechner et al., 1998, 2001; Thiers et al., 2008). Currently, the function of this innervation and neurotransmitter remain unclear. Intracellular recordings revealed that type II auditory nerves have a glutamatergic input from OHCs (Weisz et al., 2009). In this study, we found that glutamate had no effect on GJs between cochlear supporting cells (Fig. 5B&C). These data indicate that GJ-coupling between the cochlear supporting cells may be under a degree of fine neural control.

Currently, the detailed mechanisms underlying ACh uncoupling GJs between supporting cells and how changes in GJ-coupling between supporting cells affect OHC electromotility still remain unclear and need to be further studied in future. However, it is well-known that GJ channels can be closed by intracellular Ca^{2+}. We previously reported that ATP can activate purinergic P2X receptors in the cochlear supporting cells and influx Ca^{2+} to inhibit gap junctions (Zhu and Zhao, 2012). ACh regulating GJs between supporting cells may take the same mechanism. ACh receptors in the cochlea are nicotinic, formed by $\alpha9$ and $\alpha10$ subunits, which are highly Ca^{2+} permeable (Elgoyhen et

al., 1994; Vetter et al., 1999, 2007; Weisstaub et al., 2002; Gomez-Casati et al., 2005; Lustig, 2006; Lipovsek et al., 2012). ACh receptors have expression in the cochlear supporting cells and are positive to AChRα9-labeling (Fig. 1F&G). When they are activated, Ca^{2+} ions can flux into the supporting cells and consequently inhibit GJs. Indeed, although ACh-evoked inward current was fast (Figs. 2 and S1), the effect on GJ permeability was relatively slower (Fig. 6). Thus, ACh may open ACh receptors inducing Ca^{2+} influx, which could close GJ channels between the supporting cells consequently and produce long-term effects.

The controllable GJ coupling between the cochlear supporting cells may be dictated by the needs of normal hearing. We previously reported that gap junctions between supporting cells can mediate OHC electromotility (Yu and Zhao, 2009; Zhu et al., 2013) and has a critical role in active cochlear amplification and hearing (Zhu et al., 2013; Zong et al., 2017). It is well-known that the MOC efferent system can directly inhibit OHC function and reduce active cochlear amplification to reduce hearing sensitivity and provide protection from noise trauma (Eybalin, 1993; Guinan, 2006). In this study, we found that ACh reduced GJ-coupling between supporting cells (Figs. 3-4) and shifted OHC electromotility (Fig. 5) as direct effect of ACh on OHCs (Fig. S3), indicating that this supporting cell GJ-mediated pathway could enhance MOC inhibitory effect on OHCs. Moreover, deficiency of this supporting cell GJ-mediated pathway induced the reduction of hearing sensitivity (Figs. 6 and S4) and increased susceptibility to noise (Fig. 7). These data further indicate that this supporting cell GJ-mediated pathway plays an important role in the cochlear efferent function, in particular, in the protection from noise

trauma. In addition, inner ear GJs have important role in many aspects of cochlear function (Wingard and Zhao, 2015; Zhu et al., 2015). Thus, the cochlear efferent system can control inner ear GJs (Figs. 3&4) and cause a broader range of effects than that previously thought.

Materials and Methods

Animal selection and preparation

Multiple recordings and assessments, including histological examination with confocal microscopy, patch clamp electrophysiological recording, FRAP, in vivo electrophysiological recording, noise exposure, and transgenic mouse model, were used in this study. Most of electrophysiological recording were performed in adult guinea pigs (250-400 g), since it is easily to obtain large number of the cochlear supporting cells and OHCs, in particular, OHC-DC pairs. Most of histological and in vivo examinations were performed in mice, since most of transgenic animal models are mice. However, we also did some of electrophysiological recording in mice to verify the ACh responses in the cochlear supporting cells (e.g., Figs. 3, S1, and S2).

For targeted deletion of Cx26 in outer supporting cells, $Cx26^{loxP/loxP}$ transgenic mice (EM00245, European Mouse Mutant Archive) were crossed with mice of the *Prox1-CreER*^{T2} Cre line (Stock No. 022075, Jackson Laboratory, USA). As we previously reported (Zhu et al., 2013; Zong et al., 2017), Tamoxifen (T5648, Sigma-Aldrich, St. Louis, MO) was administrated to all litters at postnatal day 0 (P0) by intraperitoneal injection (0.5 mg/10g x 3 days). WT littermates were used as control. All experimental procedures were conducted in accordance with the policies of the University of Kentucky Animal Care & Use Committee.

Cochlear sensory epithelium and cell isolation

As we previously reported (Zhao and Yu, 2006; Yu and Zhao, 2008, 2009; Zhu and Zhao, 2010, 2012), mice or guinea pigs were decapitated after anesthesia with pentobarbital. Then, the temporal bone was removed and the otic capsule was dissected in the normal extracellular solution (NES, 142 NaCl, 5.37 KCl, 1.47 $MgCl_2$, 2 $CaCl_2$, 10 HEPES in mM, 300 mOsm and pH 7.2). After the organ of Corti was exposed, the sensory epithelium was picked away with a sharpened needle. Then, the isolated epithelium was transferred to the recording chamber. The outer supporting cell (Deiters cell and Hensen cell) area and isolated outer supporting cells can be unequivocally identified under microscope by their own morphological shape (Zhu and Zhao, 2010, 2012). All experiments were performed at room temperature.

Immunofluorescent staining and confocal microscopy

Immunofluorescent staining was performed as described in our previous report (Zhao and Yu, 2006). The cochlear sections were fixed with 4% paraformaldehyde for 30 min. After washout, the sections were incubated in a blocking solution (10% goat serum and 1% BSA in PBS) with 0.1% Triton X-100 and then incubated with polyclonal chicken anti-neurofilament (1:500, Cat# AB5539, Millipre Corp, CA), monoclonal mouse anti-AChRα9 (1:100, Cat# sc-293282, Santa Cruz Biotech Inc, CA), monoclonal mouse anti-Sox2 (1:200, Cat# sc-365823, Santa Cruz Biotech Inc, CA), polyclonal goat anti-prestin (1:50, Cat# sc-22694, Santa Cruz Biotech Inc, CA), or monoclonal mouse anti-Cx26 (1: 400, Cat# 33-5800, Invitrogen), at 4ºC overnight. After being washed with PBS, the sections were incubated with corresponding Alexa Fluor 488-conjugated goat anti-mouse

IgG and Alexa Fluor 568-conjugated goat anti-rabbit IgG (1:500, Molecular Probes) at room temperature (23 ºC) for 1 hr to visualize labeling.

After mounting on the glass slide, the stained epithelia were observed under a Nikon A1R confocal microscope system with Nikon 60x or 100x Plan Apro oil objective. Serial sections were scanned along the z-axis from the bottom to apical surface of the epithelium with a 0.25 μm step. NIS Elements AR Analysis software (Nikon) was used for constructing 3D image from z-stack section.

Patch-clamp recording and input capacitance measurement

The isolated cells were continuously perfused with the NES (0.5 mL/min). Single dissociated cochlear supporting cell was selected and recorded under the whole-cell configuration using an Axopatch 200B patch clamp amplifier (Molecular Devices, CA, USA) (Yu and Zhao, 2009; Zhu and Zhao, 2010). Patch pipettes were filled with an intracellular solution that contained (in mM) 140 KCl, 5 EGTA, 2 $MgCl_2$, and 10 HEPES, pH 7.2 with initial resistance of 2.5-3.5 MΩ in bath solution. Data were collected by jClamp software (SciSoft, New Haven, CT, USA). The signal was filtered by a 4-pole low-pass Bessel filter with a cut-off frequency of 2 kHz and digitized utilizing a Digidata 1322A (Molecular Devices, CA, USA).

Gap junctional coupling between cells was monitored by input capacitance (C_{in}) (Zhao and Santos-Sacchi, 1998; Zhu and Zhao, 2012). C_{in} was continually recorded online at 1-3 Hz from the transient charge induced by small (-10 mV) test pulses with

duration of 18X the time constant at the holding potential. The transient charge was calculated from the integration of capacitance current with time (Zhao and Santos-Sacchi, 1998). Membrane potential (V_m) was corrected for pipette series resistance (R_s).

Double patch clamp recording and OHC electromotility nonlinear capacitance measurement

Double patch clamp recording was performed by use of Axopatch 700A (Molecular Devices, CA, USA). One pipette was patched at the DC and another patch pipette was patched at the basal nuclear pole of the OHC under a whole-cell configuration by using jClamp (SciSoft, New Haven, CT, USA). The OHC electromotility associated NLC was measured with a two-sinusoidal wave voltage stimulus in jClamp (Zhao et al., 2005; Yu and Zhao, 2008, 2009). This voltage stimulus was composed of a ramp command (-150 mV to +150 mV) summed with two sinusoidal commands (f_1=390.6 Hz, f_2=781.3 Hz, 25 mV peak to peak). The signal was filtered by a 4-pole low-pass Bessel filter with a cut-off frequency of 10 kHz. The capacitance was calculated by admittance analysis of the current response. The peak of NLC and the voltage corresponding to the peak capacitance (V_{pk}) were also continuously recorded by a phase-tracking technique (sampling rate: 4/s, tracking-step: 0.25 mV) (Zhao et al., 2005; Yu and Zhao, 2008, 2009).

Data analysis was performed with jClamp and MATLAB (Zhao and Santos-Sacchi, 1999; Yu and Zhao, 2008, 2009). The voltage-dependent NLC was fitted to the first derivative of a two-state Boltzmann function:

$$C_m = NLC + C_{lin} = Q_{\max}\frac{ze}{kT}\frac{\exp\left(\frac{-ze(V_m - V_{pk})}{kT}\right)}{\left(1+\exp\left(\frac{-ze(V_m - V_{pk})}{kT}\right)\right)^2} + C_{lin} \qquad (1)$$

where Q_{max} is the maximum charge transferred, V_{pk} is the potential that corresponds to the peak of NLC and also has an equal charge distribution, z is the number of elementary charge (e), k is Boltzmann's constant, T is the absolute temperature and C_{lin} is the cell membrane capacitance. Curve fitting and figure plotting was performed with SigmaPlot software. Membrane potential (V_m) was corrected for pipette series resistance (R_s).

Fluorescence recovery after photobleaching (FRAP)

The freshly isolated cochlear epithelium or cells were incubated in 10 μM Carboxy SNARF-1 AM (C-1271, Molecular Probes) at room temperature for 15-30 min, protected from light. Then, the incubated tissues or cells were continuously perfused with the NES for 30-45 min to remove the residual dye and allow completion of the hydrolysis of AM ester prior to measurement.

FRAP measuring was performed by use of a laser scanning confocal system. Prior to laser bleaching, the fluorescence image of the selected area in the cochlear sensory epithelium was scanned and saved. Then, a laser beam (the laser power is nominally about 50 μW) illuminated a selected cell for 20 seconds to bleach the fluorescence. After bleaching, the fluorescent images were taken at 0, 5, 15, 30, 60, 120, 210 and 330 s to measure the recovery. The intensity of fluorescence of the bleached cell was measured off-line by use of ImageJ software (NIH, Bethesda, MD) and normalized to the

fluorescent intensity in the same cell prior to bleaching. The fluorescence recovery data were fitted by:

$$F(t) = F(\infty) - \Delta F(0)\, e^{-t/\tau} \qquad (1)$$

where $F(\infty)$ is the fluorescence signal of the bleached cell at $t = \infty$, $\Delta F(0)$ is the initial fluorescence change due to the bleaching, and τ is the recovery time constant.

Noise exposure

Mice were awake in a small cage under loud-speakers in a sound-proof chamber and exposed to white-noise (96 dB SPL) for 2 hr, one time. Sound pressure level and spectrum in the cage were measured prior to placement of the animal.

Auditory brainstem response and DPOAE recording

As we previously reported (Zhu et al., 2013, 2015), the ABR was recorded by use of a Tucker-Davis ABR & DPOAE workstation with ES-1 high frequency speaker (Tucker-Davis Tech. Alachua, FL). Mice were anesthetized by intraperitoneal injection with a mixture of ketamine and xylazine (8.5 ml saline+1 ml Ketamine+0.55 ml Xylazine, 0.1 ml/10 g). Body temperature was maintained at 37–38°C. ABR was measured by clicks and tone bursts (8 – 40 kHz) from 80 to 10 dB SPL in a 5 dB step. The ABR threshold was determined by the lowest level at which an ABR can be recognized. If mice had severe hearing loss, the ABR test from 110 to 70 dB SPL was added.

DPOAE was recorded as described by our previous reports (Zhu et al., 2013, 2015). Two pure tones (f_1 and f_2) were simultaneously delivered into the ear through two plastic

tubes coupled to two high-frequency speakers (EC-1, Tucker-Davis Tech. Alachua, FL). The test frequencies were presented by a geometric mean of f_1 and f_2 [$f_0 = (f_1 \times f_2)^{1/2}$] from f_0=4 to 20 kHz. The ratio of f_2 versus f_1 (f_2/f_1) was 1.22. The intensity of f_1 was set at 5 dB SPL higher than that of f_2. One hundred fifty responses were averaged. A cubic distortion component of $2f_1$-f_2 in DPOAEs was measured.

Chemicals and data processing

All chemicals were purchased from Sigma Chemical Company (St. Louis, U.S.A.). Chemicals were delivered by a Y-tube perfusion system (Yu and Zhao, 2008, 2009; Zhu and Zhao, 2010). Data analyses were performed by MATLAB. Data were expressed as mean ± s.e.m. unless otherwise indicated in text and plotted by SigmaPlot (SPSS Inc. Chicago, IL). The statistical analyses were performed by SPSS v18.0 (SPSS Inc. Chicago, IL).

Acknowledgments:

We thank Dr. Michael Bennett for valuable comments on the earlier version of this manuscript. This work was supported by NIH R01 DC 017025 and R56 DC 016585 to HBZ.

Author Contributions:

HBZ conceived the general framework of this study. YZ, LML, LM, YN, CL, JC, YMZ, and HBZ performed the experiments. HBZ, NY, YZ, and LML analyzed data. HBZ wrote the paper. All authors reviewed the manuscript and provided the input.

Conflict of Interest:

The authors declare no competing financial interests.

References

Ashmore J (2008) Cochlear outer hair cell motility. Physiol Rev 88: 173–210.

Boero LE, Castagna VC, Di Guilmi MN, Goutman JD, Elgoyhen AB, Gómez-Casati ME. (2018) Enhancement of the medial olivocochlear system prevents hidden hearing loss. J Neurosci. 38: 7440-7451. doi: 10.1523/JNEUROSCI.0363-18.2018.

Brownell WE, Bader CR, Bertrand D, Ribaupierre Y (1985) Evoked mechanical responses of isolated cochlear outer hair cells. Science 227: 194-196.

Bruce LL, Christensen MA, Warr WB. (2000) Postnatal development of efferent synapses in the rat cochlea. J Comp Neurol. 423: 532-548.

Burgess BJ, Adams JC, Nadol JB. (1997) Morphologic evidence for innervation of Deiters' and Hensen's cells in the guinea pig. Hear Res. 108: 74-82.

Castillo FJ, Castillo I. (2011) The DFNB1 subtype of autosomal recessive non-syndromic hearing impairment. Front Biosci. 17: 3252-3274.

Chen GD, Zhao HB. (2007) Effects of intense noise exposure on the outer hair cell plasma membrane fluidity. Hear Res. 226: 14-21.

Chan DK, Chang KW. (2014) GJB2-associated hearing loss: systematic review of worldwide prevalence, genotype, and auditory phenotype. Laryngoscope. 124: E34-53. doi: 10.1002/lary.24332.

Ciuman RR. (2010) The efferent system or olivocochlear function bundle - fine regulator and protector of hearing perception. Int J Biomed Sci. 6: 276-288.

Clause A, Lauer AM, Kandler K. (2017) Mice lacking the alpha9 subunit of the nicotinic acetylcholine receptor exhibit deficits in frequency difference limens and sound localization. Front Cell Neurosci. 11:167. doi: 10.3389/fncel.2017.00167.

Elgoyhen AB, Johnson DS, Boulter J, Vetter DE, Heinemann S. (1994) Alpha 9: an acetylcholine receptor with novel pharmacological properties expressed in rat cochlear hair cells. Cell 79: 705-715.

Eybalin M. (1993) Neurotransmitters and neuromodulators of the mammalian cochlea. Physiol Rev. 73: 309-373.

Fechner FP, Burgess BJ, Adams JC, Liberman MC, Nadol JB Jr. (1998) Dense innervation of Deiters' and Hensen's cells persists after chronic deefferentation of guinea pig cochleas. J Comp Neurol. 400: 299-309.

Fechner FP, Nadol JB JR, Burgess BJ, Brown MC. (2001) Innervation of supporting cells in the apical turns of the guinea pig cochlea is from type II afferent fibers. J Comp Neurol. 429: 289-298.

Forge A, Becker D, Casalotti S, Edwards J, Marziano N, Nevill G. (2003) Gap junctions in the inner ear: comparison of distribution patterns in different vertebrates and assessement of connexin composition in mammals. J Comp Neurol. 467: 207-231.

Gómez-Casati ME, Fuchs PA, Elgoyhen AB, Katz E. (2005) Biophysical and pharmacological characterization of nicotinic cholinergic receptors in rat cochlear inner hair cells. J Physiol. 566: 103-118.

Guinan JJ. (2006) Olivocochlear efferents: anatomy, physiology, function, and the measurement of efferent effects in humans. Ear Hear. 27: 589-607.

Iwasa KH. (1993) Effect of stress on the membrane capacitance of the auditory outer hair cell. Biophys J. 65:492-498.

Kakehata S, Santos-Sacchi J (1995) Membrane tension directly shifts voltage dependence of outer hair cell motility and associated gating charge. Biophys J. 68: 2190-2197.

Kikuchi T, Kimura RS, Paul DL, Adams JC. (1995) Gap junctions in the rat cochlea: immunohistochemical and ultrastructural analysis. Anat Embryol 191: 101-118.

Liberman MC. (1980) Morphological differences among radial afferent fibers in the cat cochlea: An electron-microscopic study of serial sections. Hear Res 3: 45-63.

Liberman MC, Dodds LW, Pierce S. (1990) Afferent and efferent innervation of the cat cochlea: quantitative analysis with light and electron microscopy. J Comp Neurol. 301: 443-460.

Liberman MC, Gao J, He DZ, Wu X, Jia S, Zuo J. (2002) Prestin is required for electromotility of the outer hair cell and for the cochlear amplifier. Nature 419:300-304.

Lipovsek M, Im GJ, Franchini LF, Pisciottano F, Katz E, Fuchs PA, Elgoyhen AB. (2012) Phylogenetic differences in calcium permeability of the auditory hair cell cholinergic nicotinic receptor. Proc Natl Acad Sci USA. 109: 4308-4313.

Liu YP, Zhao HB. (2008) Cellular characterization of Connexin26 and Connnexin30 expression in the cochlear lateral wall. Cell Tissue Res. 333: 395-403.

Lustig LR. (2006) Nicotinic acetylcholine receptor structure and function in the efferent auditory system. Anat Rec A Discov Mol Cell Evol Biol. 288: 424-434.

Maison SF, Liu XP, Eatock RA, Sibley DR, Grandy DK, Liberman MC. (2012) Dopaminergic signaling in the cochlea: receptor expression patterns and deletion phenotypes. J Neurosci. 32: 344-355. doi: 10.1523/JNEUROSCI.4720-11.2012.

Matsubara A, Laake JH, Davanger S, Usami S, Ottersen OP. (1996) Organization of AMPA receptor subunits at a glutamate synapse: quantitative immunogold analysis of hair cell synapses in the rat organ of Corti. J Neurosci. 16: 4457-4467.

Mei L, Chen J, Zong L, Zhu Y, Liang C, Jones RO, Zhao HB. (2017) A deafness mechanism of digenic Cx26 (GJB2) and Cx30 (GJB6) mutations: Reduction of endocochlear potential by impairment of heterogeneous gap junctional function in the cochlear lateral wall. Neurobiol Dis. 108: 195-203. doi: 10.1016/j.nbd.2017.08.002.

Nadol JB, Burgess BJ. (1994) Supranuclear efferent synapses on outer hair cells and Deiters' cells in the human organ of Corti. Hear Res. 81: 49-56.

Rabbitt RD. (2020) The cochlear outer hair cell speed paradox. Proc Natl Acad Sci U S A. 117(36):21880-21888. doi: 10.1073/pnas.2003838117. Epub 2020 Aug 26.

Simmons DD. (2002) Development of the inner ear efferent system across vertebrate species. J Neurobiol. 53: 228-250.

Stopp PE, Comis SD. (1979) Relationship of centrifugal fibers to 'supporting' cells. Arch Otorhinolaryn. 224: 11-15.

Thiers FA, Nadol JB, Jr., Liberman MC (2008) Reciprocal synapses between outer hair cells and their afferent terminals: Evidence for a local neural network in the mammalian cochlea. J Assoc Res Otolaryngol 9: 477-489.

Vetter DE, Katz E, Maison SF, Taranda J, Turcan S, Ballestero J, Liberman MC, Elgoyhen AB, Boulter J. (2007) The alpha10 nicotinic acetylcholine receptor subunit is

required for normal synaptic function and integrity of the olivocochlear system. Proc Natl Acad Sci USA 104: 20594-20599.

Vetter DE, Liberman MC, Mann J, Barhanin J, Boulter J, Brown MC, Saffiote-Kolman J, Heinemann SF, Elgoyhen AB. (1999) Role of alpha9 nicotinic ACh receptor subunits in the development and function of cochlear efferent innervation. Neuron 23: 93-103.

Weisstaub N, Vetter DE, Elgoyhen AB, Katz E. (2002) The alpha9alpha10 nicotinic acetylcholine receptor is permeable to and is modulated by divalent cations. Hear Res. 167: 122-135.

Weisz C, Glowatzki E, Fuchs P. (2009) The postsynaptic function of type II cochlear afferents. Nature 461:1126-1129.

Wingard JC, Zhao HB. (2015) Cellular and deafness mechanisms underlying connexin mutation-induced hearing loss - A common hereditary deafness. Front Cell Neurosci. 9: 202. doi: 10.3389/fncel.2015.00202.

Wright CG, Preston RE. (1976) Efferent nerve fibers associated with the outermost supporting cells of the organ of Corti in the guinea pig. Acta Otolaryngol. 82: 41-47.

Yu N, Zhao HB. (2009) Modulation of outer hair cell electromotility by cochlear supporting cells and gap junctions. PLoS One 4(11): e7923.

Zhao HB, Santos-Sacchi J. (1998) Effect of membrane tension on gap junctional conductance of supporting cells in Corti's organ. J Gen Physiol. 112: 447-455.

Zhao HB, Santos-Sacchi J. (1999) Auditory collusion and a coupled couple of outer hair cells. Nature 399: 359-362.

Zhao HB, Yu N. (2006) Distinct and gradient distributions of connexin26 and connexin30 in the cochlear sensory epithelium of guinea pigs. J Comp Neurol. 499: 506-518.

Zheng J, Shen W, He DZ, Long KB, Madison LD, Dallos P. (2000) Prestin is the motor protein of cochlear outer hair cells. Nature 405:149-155.

Zhu Y, Chen J, Liang C, Zong L, Chen J, Jones RO, Zhao HB. (2015) Connexin26 (GJB2) deficiency reduces active cochlear amplification leading to late-onset hearing loss. Neuroscience 284: 719-729.

Zhu Y, Liang C, Chen J, Zong L, Chen GD, Zhao HB. (2013) Active cochlear amplification is dependent on supporting cell gap junctions. Nat Commun. 4: 1786. doi: 10.1038/ncomms2806.

Zhu Y, Zhao HB. (2010) ATP-mediated potassium recycling in the cochlear supporting cells. Purinergic Signal. 6: 221-229.

Zhu Y, Zhao HB. (2012) ATP activates P2X receptors to mediate gap junctional coupling in the cochlea. Biochem Biophys Res Commun. 426: 528-532.

Zhu Y, Zong L, Mei L, Zhao HB. (2015) Connexin26 gap junction mediates miRNA intercellular genetic communication in the cochlea and is required for inner ear development. Sci Rep. 5: 15647. doi: 10.1038/srep15647.

Zong L, Chen J, Zhu Y, Zhao HB. (2017) Progressive age-dependence and frequency difference in the effect of gap junctions on active cochlear amplification and hearing. Biochem Biophys Res Commun. 489: 223-227. doi: 10.1016/j.bbrc.2017.05.137.

Figure legends

Fig. 1. Innervation of the medial olivocochlear (MOC) efferent nerves and ACh receptor (AChR) expression in the cochlear supporting cells in mice. **A:** Cross-section view of the cochlea. A green arrow indicated MOC fibers cross the cochlear tunnel which is indicated by a white star. IHC: inner hair cell, OHC: outer hair cell, DC: Deiters cell, HC: Hensen cell, PC: pillar cell. **B:** Confocal image of immunofluorescent staining of the cochlear sensory epithelium for neurofilament (NF, green), prestin (red), and Sox2 (purple) in whole-mount preparation. The MOC fibers, OHCs, and supporting cells (SCs) are labeled by NF (green), prestin (red), and Sox2 (purple), respectively. MOC fibers are clearly visible in OHC and SC areas. **C:** The surface-view at the SC layer without OHC layer in the confocal image. Innervations of MOC fibers with SCs are clearly visible. **D-E:** The cross-section view in 3D images of the cochlear sensory epithelium constructed from z-stack of serial confocal scanning images. The branches of the MOC fibers projecting to DCs, HCs, and PCs are clearly visible. While arrowheads in panel D and E indicate the MOC branch projecting to the DC and PC, respectively. **F-G:** AChR expression at the OHCs and supporting cells. The images were the cross-section view of 3D images constructed from z-stack of confocal scanning. AChR and NF are labeled by green and red colors, respectively, in immunofluorescent staining. Triangles with green color indicate AChR expression at the OHC basal pole and white arrowheads indicate expression of AChR at DCs and HCs. Scale bar: 20 μm in **A-C**; 10 μm in **D-G**.

Fig. 2. ACh-evoked current response in Deiters cells (DCs) in guinea pigs. **A**: A captured image of patch clamp recording at a DC. **B:** An inward current elicited by 0.5 mM ACh

in a DC. The membrane potential was clamped at -80 mV. A horizontal bar represents the application of 0.5 mM ACh. **C:** Current traces in a DC were evoked by voltage-step stimulation at the application of 0.5 mM ACh and control (pre-application). ACh-evoked response was obtained by subtracting the control response from the response at the ACh application. **D**: Current-voltage (I-V) curves at the application of 0.5 mM ACh and control. The I-V relations were plotted by average values of the steady-state current responses in last 20 ms of the voltage step stimulation. The ACh-evoked I-V curve was obtained by subtracting the control currents from the currents recorded at the application of ACh. **E:** Dose curve of ACh-evoked current in DCs. The ACh-evoked currents were measured at cells held at -80 mV. The smooth line represents data fitting to a Hill's function: $I=a * C^n/(K^n + C^n)$, where n=1.67 (Hill coefficient) and K=91.8 μM (EC_{50}) for ACh.

Fig. 3. ACh uncouples GJs between the cochlear supporting cells. The coupling of GJs between supporting cells was measured by input capacitance (C_{in}). **A-B:** ACh-induced GJ uncoupling between mouse supporting cells. Panel A shows the reversible uncoupling of ACh on 2 mouse DCs. After application of 0.5 mM ACh, C_{in} was reduced to a half value. The uncoupling effect is reversible. After stop of ACh perfusion, C_{in} was returned to the coupled level. Panel B shows step-changes in C_{in} for uncoupling of GJs among three-coupled HCs. **C-D:** ACh-induced uncoupling of GJs between two guinea pig DCs. After closing GJs between cells under treatment of 0.5 mM ACh, C_{in} was reduced to the half value.

Fig. 4. The effect of neurotransmitters of ACh and glutamate on GJ permeability between outer supporting cells (DCs and HCs) measured by FRAP in guinea pigs. **A:** Fluorescent images of cochlear sensory epithelium in the HC area and fluorescence recovery after photobleaching by laser zapping (indicated by a red arrow). Scale bar: 10 μm. **B:** Fluorescence recovery of outer supporting cells at ACh (0.5 mM) or glutamate (0.2 mM) treatment. The data points were averaged from different cells measured at 10 -20 minutes after treatment of ACh or glutamate. Solid lines represent exponential fitting to data. **C:** The recovery time constant (τ) of FRAP. ACh but not glutamate significantly increased the recovery time constant of FRAP, i.e., reduced GJ permeability. **: $P<0.001$, one-way ANOVA with a Bonferroni correction. **D:** Dynamic changes of GJ permeability in cochlear supporting cells for application of ACh. The time constants of FRAP were measured pre- and post-application of 0.5 mM ACh. The black circles and solid line represent the average value from three measurements. The red line represents exponential fitting. The time constant of the fitting is 11.0 min.

Fig. 5. Influence of change in GJs between DCs on OHC electromotility in guinea pigs. **A:** A captured image of dual-patch clamp recording at a pair of DC and OHC. One patch pipette was recording at an OHC and another patch pipette was recorded at DCs. **B-D:** Uncoupling of GJs between DCs induced current changes and influence on OHC electromotility. GJs between DCs were uncoupled by application of an uncoupling agent 10 mM octanol. C_{in} in panel B recorded from DCs' patch pipette was reversibly reduced to a half value, indicating uncoupling of GJs between cells. Panel C and D show GJ-uncoupling induced large current changes in DCs and shift of OHC electromotility

associated nonlinear capacitance (NLC) in the OHC, respectively. Smooth lines in panel D represent NLC fitted by Boltzmann function. The parameters of fitting are Q_{max}=3.08 & 3.09 pC, z=0.87 & 0.82, V_{pk}=-47.9 & -58.4 mV, and C_{lin}=22.4 & 22.2 pF for DCs under GJ-coupling and -uncoupling, respectively. **E:** Simulative current changes in DCs by current injection in DCs through the DC patch pipette induced changes in OHC NLC in a DC-OHC pair. DCs were injected with different currents with holding at different holding currents and OHC electromotility associated NLC was simultaneously recorded by a voltage ramp with sinusoidal voltage. Injection of negative current in DCs led NLC left-shifting in the OHC. V_{pk} of NLC was -86.0, -81.0, -77.5, -74.8, and -72.5 mV for DCs holding at -4, -2, 0, 2, 4 nA, respectively.

Fig. 6. Deficiency of the GJ-mediated efferent pathway by targeted-deletion of Cx26 expression in DCs declines active cochlear amplification and regulation. Wild-type (WT) littermates served as control. Mice were postnatal day 45 old. **A:** Targeted-deletion of Cx26 in DCs. A white arrow indicates lack of Cx26 labeling in the DC area in Cx26 conditional-knockout (cKO) mice in immunofluorescent staining for Cx26 (green). OHCs were visualized by prestin staining (red). Scale bars: 50 μm. **B:** Spectrum of acoustic emission recorded from Cx26 cKO mice and WT mice. Insets: Large scale plotting of $2f_1$-f_2 and f_1 peaks. The peak of DPOAE ($2f_1$-f_2) in Cx26 cKO mice was reduced but f_1 and f_2 peaks remained the same as those in WT mice. f_0=20 kHz, I_1/I_2=60/55 dB SPL. **C:** Reduction of DPOAE in Cx26 cKO mice in I/O plot. **D:** I-O function of DP gain ($2f_1$-f_2 re: f_1) in Cx26 cKO mice and WT mice. DP gain in WT mice was almost flat, whereas

the DP gain in Cx26 cKO mice decreased as sound intensity increased. **: $P < 0.01$, two-tail t test.

Fig. 7. Deficiency of GJ-mediated control pathway increases susceptibility to noise in mice. Mice were exposed to 96 dB SPL while-noise for 2-hr, one time. Black vertical arrows indicate the noise-exposure day, which was defined as post-exposure day 0. Control mice were not exposed to noise. DPOAE ($2f_1$-f_2) was measured at f_0=20 kHz, I_1/I_2=60/55 dB SPL. ABR thresholds were measured by 16 kHz tone-bursts and normalized to the pre-noise exposure level. **A-B:** Noise-induced DPOAE and ABR threshold changes in Cx26 cKO mice. A blue arrow in panel A indicates that DPOAE was reduced to the minimum level at post-exposure day 3 in Cx26 cKO mice. DPOAE and ABR thresholds in Cx26 cKO mice were not completely recovered after noise exposure. **C-D:** DPOAE and ABR threshold changes in WT mice for noise exposure. DPOAE and ABR thresholds were completely recovered at post-exposure day 28.

Fig. 8. Schematic drawing for a new supporting cell GJ-mediated control pathway of the MOC efferent system to regulate OHC electromotility. **A:** Schematic drawing of MOC nerve innervations in OHCs and supporting cells. **B:** Schematic drawing of MOC efferent pathways to control OHC electromotility. A dashed-line rectangle indicates a new pathway of the MOC efferent system via the regulation of supporting cell GJs to control OHC electromotility. CC: Claudius cell; DC: Deiters cell; GJ: gap junction; HC: Hensen cell; PC: pillar cell; SC: supporting cell.

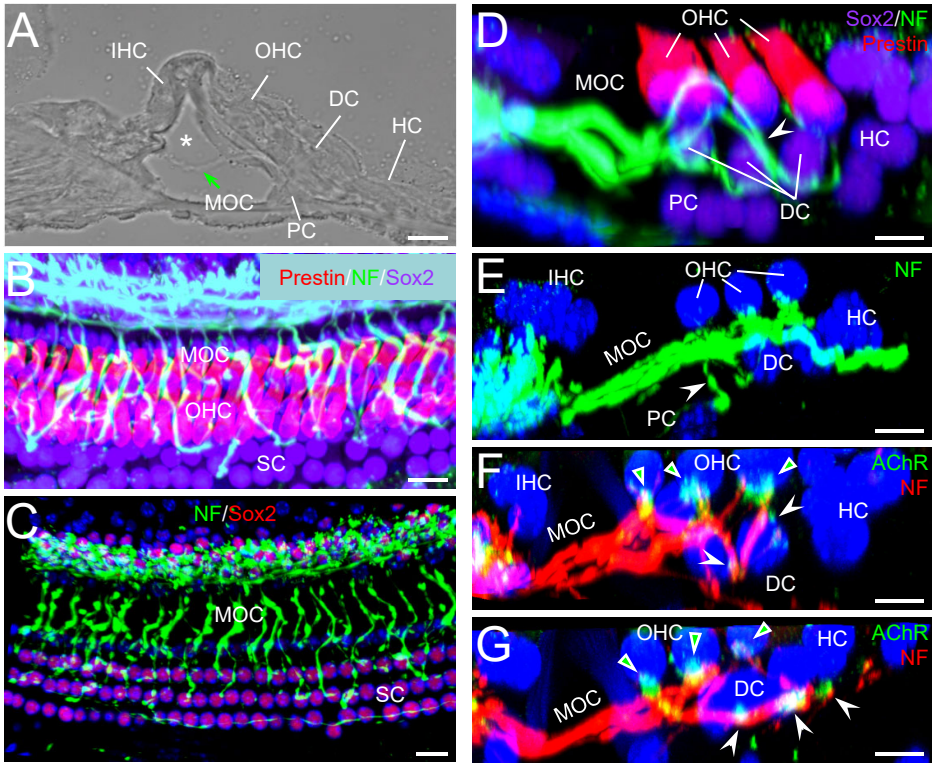

Fig. 1. Innervation of the medial olivocochlear (MOC) efferent nerves and ACh receptor (AChR) expression in the cochlear supporting cells in mice. **A:** Cross-section view of the cochlea. A green arrow indicated MOC fibers cross the cochlear tunnel which is indicated by a white star. IHC: inner hair cell, OHC: outer hair cell, DC: Deiters cell, HC: Hensen cell, PC: pillar cell. **B:** Confocal image of immunofluorescent staining of the cochlear sensory epithelium for neurofilament (NF, green), prestin (red), and Sox2 (purple) in whole-mount preparation. The MOC fibers, OHCs, and supporting cells (SCs) are labeled by NF (green), prestin (red), and Sox2 (purple), respectively. MOC fibers are clearly visible in OHC and SC areas. **C:** The surface-view at the SC layer without OHC layer in the confocal image. Innervations of MOC fibers with SCs are clearly visible. **D-E:** The cross-section view in 3D images of the cochlear sensory epithelium constructed from z-stack of serial confocal scanning images. The branches of the MOC fibers projecting to DCs, HCs, and PCs are clearly visible. While arrowheads in panel D and E indicate the MOC branch projecting to the DC and PC, respectively. **F-G:** AChR expression at the OHCs and supporting cells. The images were the cross-section view of 3D images constructed from z-stack of confocal scanning. AChR and NF are labeled by green and red colors, respectively, in immunofluorescent staining. Triangles with green color indicate AChR expression at the OHC basal pole and white arrowheads indicate expression of AChR at DCs and HCs. Scale bar: 20 μm in **A-C**; 10 μm in **D-G**.

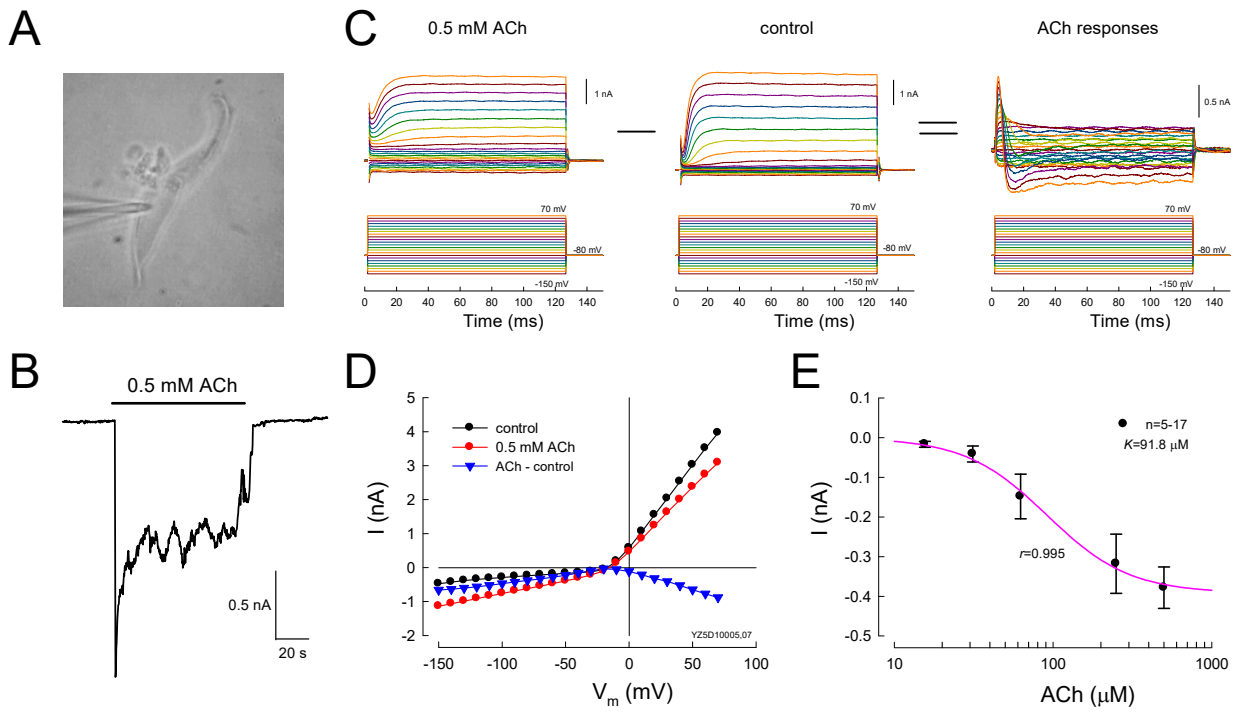

Fig. 2. ACh-evoked current response in Deiters cells (DCs) in guinea pigs. **A**: A captured image of patch clamp recording at a DC. **B:** An inward current elicited by 0.5 mM ACh in a DC. The membrane potential was clamped at -80 mV. A horizontal bar represents the application of 0.5 mM ACh. **C:** Current traces in a DC were evoked by voltage-step stimulation at the application of 0.5 mM ACh and control (pre-application). ACh-evoked response was obtained by subtracting the control response from the response at the ACh application. **D**: Current-voltage (I-V) curves at the application of 0.5 mM ACh and control. The I-V relations were plotted by average values of the steady-state current responses in last 20 ms of the voltage step stimulation. The ACh-evoked I-V curve was obtained by subtracting the control currents from the currents recorded at the application of ACh. **E:** Dose curve of ACh-evoked current in DCs. The ACh-evoked currents were measured at cells held at -80 mV. The smooth line represents data fitting to a Hill's function: $I=a * C^n/(K^n + C^n)$, where n=1.67 (Hill coefficient) and K=91.8 μM (EC_{50}) for ACh.

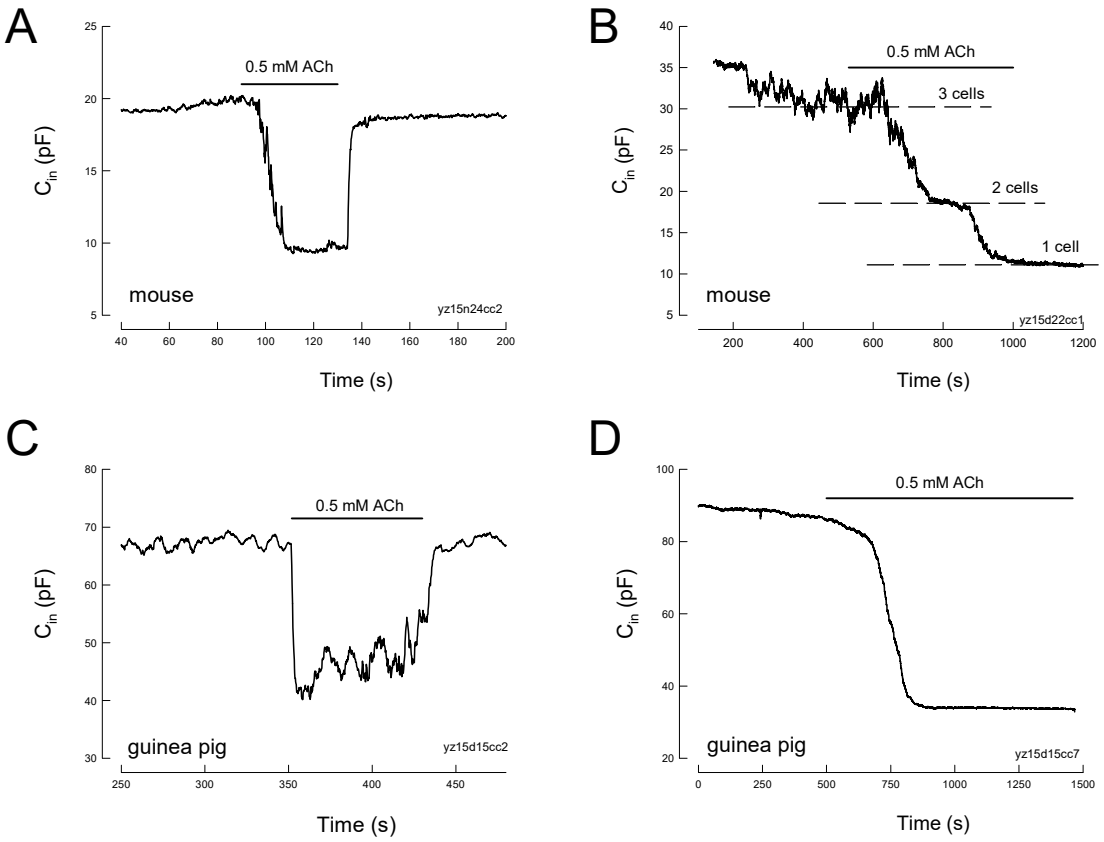

Fig. 3. ACh uncouples GJs between the cochlear supporting cells. The coupling of GJs between supporting cells was measured by input capacitance (C_{in}). **A-B:** ACh-induced GJ uncoupling between mouse supporting cells. Panel A shows the reversible uncoupling of ACh on 2 mouse DCs. After application of 0.5 mM ACh, C_{in} was reduced to a half value. The uncoupling effect is reversible. After stop of ACh perfusion, C_{in} was returned to the coupled level. Panel B shows step-changes in C_{in} for uncoupling of GJs among three-coupled HCs. **C-D:** ACh-induced uncoupling of GJs between two guinea pig DCs. After closing GJs between cells under treatment of 0.5 mM ACh, C_{in} was reduced to the half value.

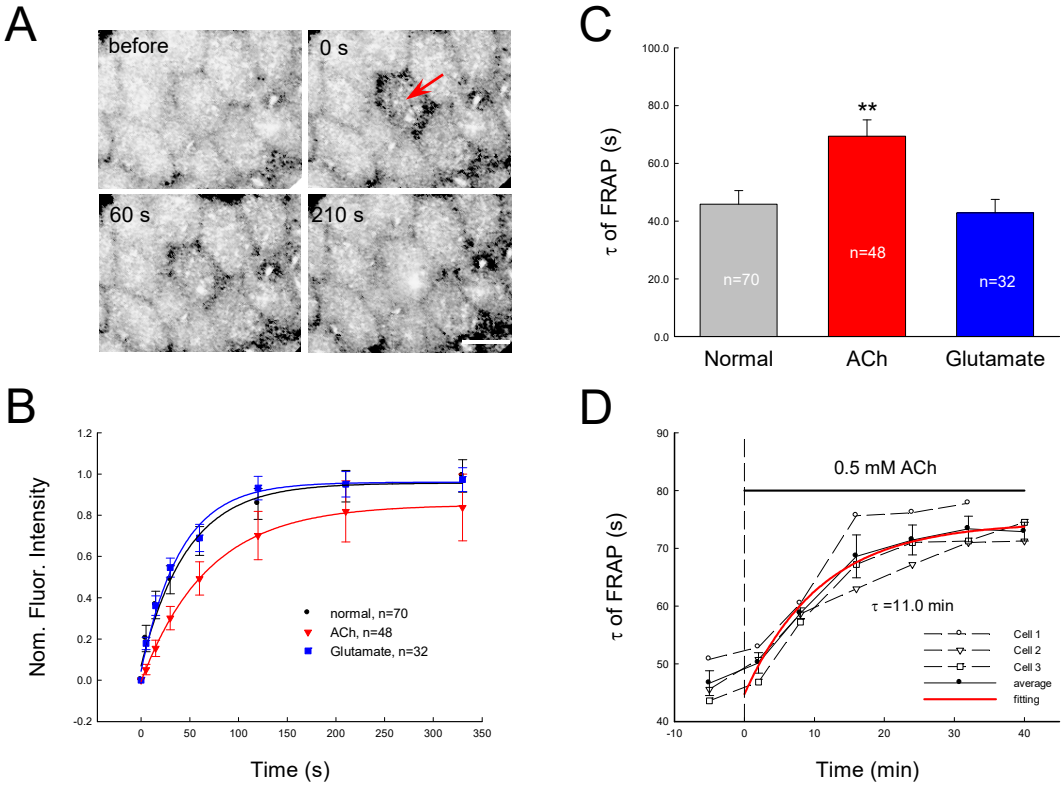

Fig. 4. The effect of neurotransmitters of ACh and glutamate on GJ permeability between outer supporting cells (DCs and HCs) measured by FRAP in guinea pigs. **A:** Fluorescent images of cochlear sensory epithelium in the HC area and fluorescence recovery after photobleaching by laser zapping (indicated by a red arrow). Scale bar: 10 μm. **B:** Fluorescence recovery of outer supporting cells at ACh (0.5 mM) or glutamate (0.2 mM) treatment. The data points were averaged from different cells measured at 10 -20 minutes after treatment of ACh or glutamate. Solid lines represent exponential fitting to data. **C:** The recovery time constant (t) of FRAP. ACh but not glutamate significantly increased the recovery time constant of FRAP, i.e., reduced GJ permeability. **: $P<0.001$, one-way ANOVA with a Bonferroni correction. **D:** Dynamic changes of GJ permeability in cochlear supporting cells for application of ACh. The time constants of FRAP were measured pre- and post-application of 0.5 mM ACh. The black circles and solid line represent the average value from three measurements. The red line represents exponential fitting. The time constant of the fitting is 11.0 min.

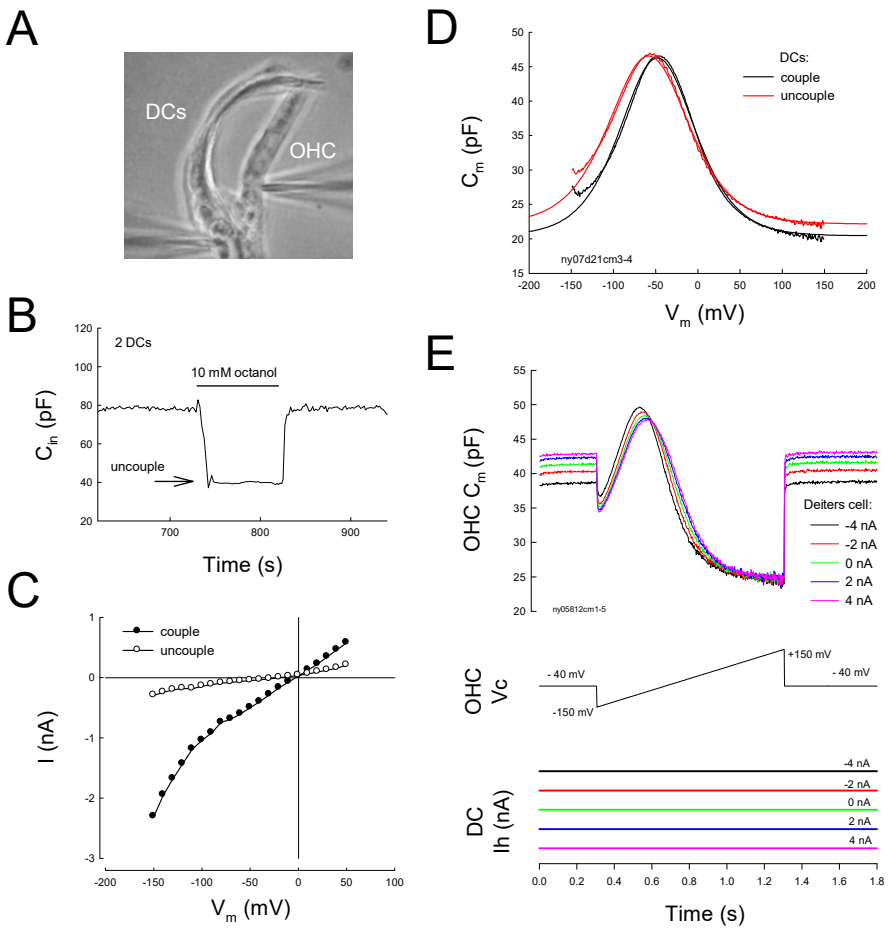

Fig. 5. Influence of change in GJs between DCs on OHC electromotility in guinea pigs. **A:** A captured image of dual-patch clamp recording at a pair of DC and OHC. One patch pipette was recording at an OHC and another patch pipette was recorded at DCs. **B-D:** Uncoupling of GJs between DCs induced current changes and influence on OHC electromotility. GJs between DCs were uncoupled by application of an uncoupling agent 10 mM octanol. C_{in} in panel B recorded from DCs' patch pipette was reversibly reduced to a half value, indicating uncoupling of GJs between cells. Panel C and D show GJ-uncoupling induced large current changes in DCs and shift of OHC electromotility associated nonlinear capacitance (NLC) in the OHC, respectively. Smooth lines in panel D represent NLC fitted by Boltzmann function. The parameters of fitting are Q_{max}=3.08 & 3.09 pC, z=0.87 & 0.82, V_{pk}=-47.9 & -58.4 mV, and C_{lin}=22.4 & 22.2 pF for DCs under GJ-coupling and -uncoupling, respectively. **E:** Simulative current changes in DCs by current injection in DCs through the DC patch pipette induced changes in OHC NLC in a DC-OHC pair. DCs were injected with different currents with holding at different holding currents and OHC electromotility associated NLC was simultaneously recorded by a voltage ramp with sinusoidal voltage. Injection of negative current in DCs led NLC left-shifting in the OHC. V_{pk} of NLC was -86.0, -81.0, -77.5, -74.8, and -72.5 mV for DCs holding at -4, -2, 0, 2, 4 nA, respectively.

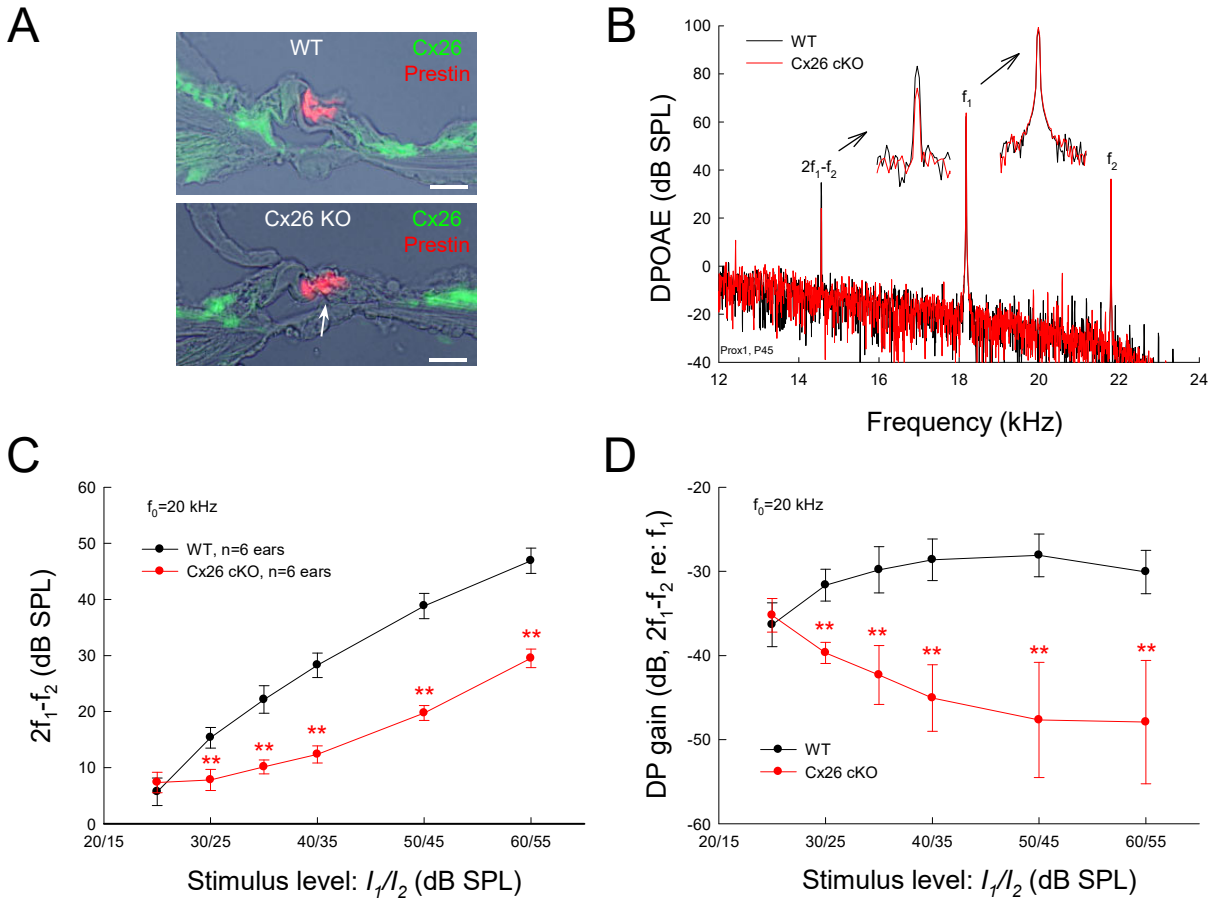

Fig. 6. Deficiency of the GJ-mediated efferent pathway by targeted-deletion of Cx26 expression in DCs declines active cochlear amplification and regulation. Wild-type (WT) littermates served as control. Mice were postnatal day 45 old. **A:** Targeted-deletion of Cx26 in DCs. A white arrow indicates lack of Cx26 labeling in the DC area in Cx26 conditional-knockout (cKO) mice in immunofluorescent staining for Cx26 (green). OHCs were visualized by prestin staining (red). Scale bars: 50 μm. **B:** Spectrum of acoustic emission recorded from Cx26 cKO mice and WT mice. Insets: Large scale plotting of $2f_1$-f_2 and f_1 peaks. The peak of DPOAE ($2f_1$-f_2) in Cx26 cKO mice was reduced but f_1 and f_2 peaks remained the same as those in WT mice. f_0=20 kHz, I_1/I_2=60/55 dB SPL. **C:** Reduction of DPOAE in Cx26 cKO mice in I/O plot. **D:** I-O function of DP gain ($2f_1$-f_2 re: f_1) in Cx26 cKO mice and WT mice. DP gain in WT mice was almost flat, whereas the DP gain in Cx26 cKO mice decreased as sound intensity increased. **: $P < 0.01$, two-tail t test.

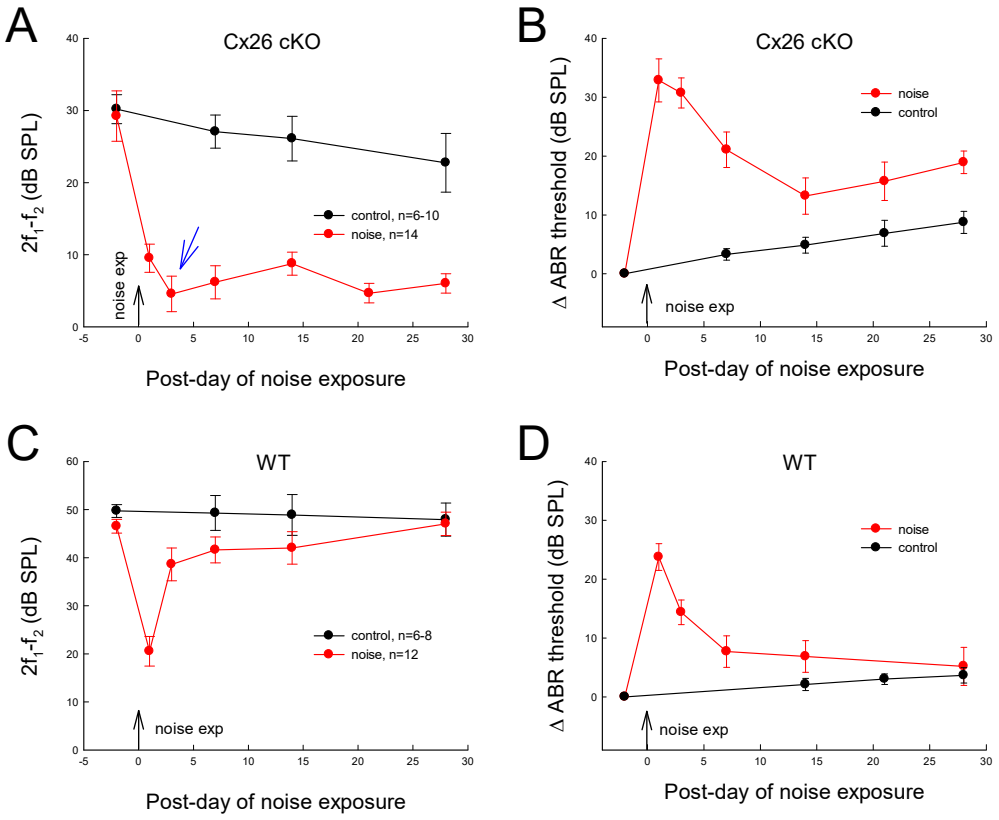

Fig. 7. Deficiency of GJ-mediated control pathway increases susceptibility to noise in mice. Mice were exposed to 96 dB SPL while-noise for 2-hr, one time. Black vertical arrows indicate the noise-exposure day, which was defined as post-exposure day 0. Control mice were not exposed to noise. DPOAE ($2f_1$-f_2) was measured at f_0=20 kHz, I_1/I_2=60/55 dB SPL. ABR thresholds were measured by 16 kHz tone-bursts and normalized to the pre-noise exposure level. **A-B:** Noise-induced DPOAE and ABR threshold changes in Cx26 cKO mice. A blue arrow in panel A indicates that DPOAE was reduced to the minimum level at post-exposure day 3 in Cx26 cKO mice. DPOAE and ABR thresholds in Cx26 cKO mice were not completely recovered after noise exposure. **C-D:** DPOAE and ABR threshold changes in WT mice for noise exposure. DPOAE and ABR thresholds were completely recovered at post-exposure day 28.

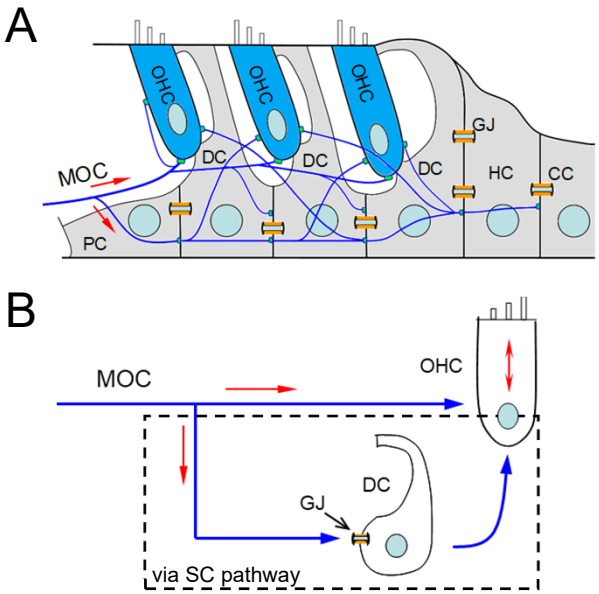

Fig. 8. Schematic drawing for a new supporting cell GJ-mediated control pathway of the MOC efferent system to regulate OHC electromotility. **A:** Schematic drawing of MOC nerve innervations in OHCs and supporting cells. **B:** Schematic drawing of MOC efferent pathways to control OHC electromotility. A dashed-line rectangle indicates a new pathway of the MOC efferent system via the regulation of supporting cell GJs to control OHC electromotility. CC: Claudius cell; DC: Deiters cell; GJ: gap junction; HC: Hensen cell; PC: pillar cell; SC: supporting cell.

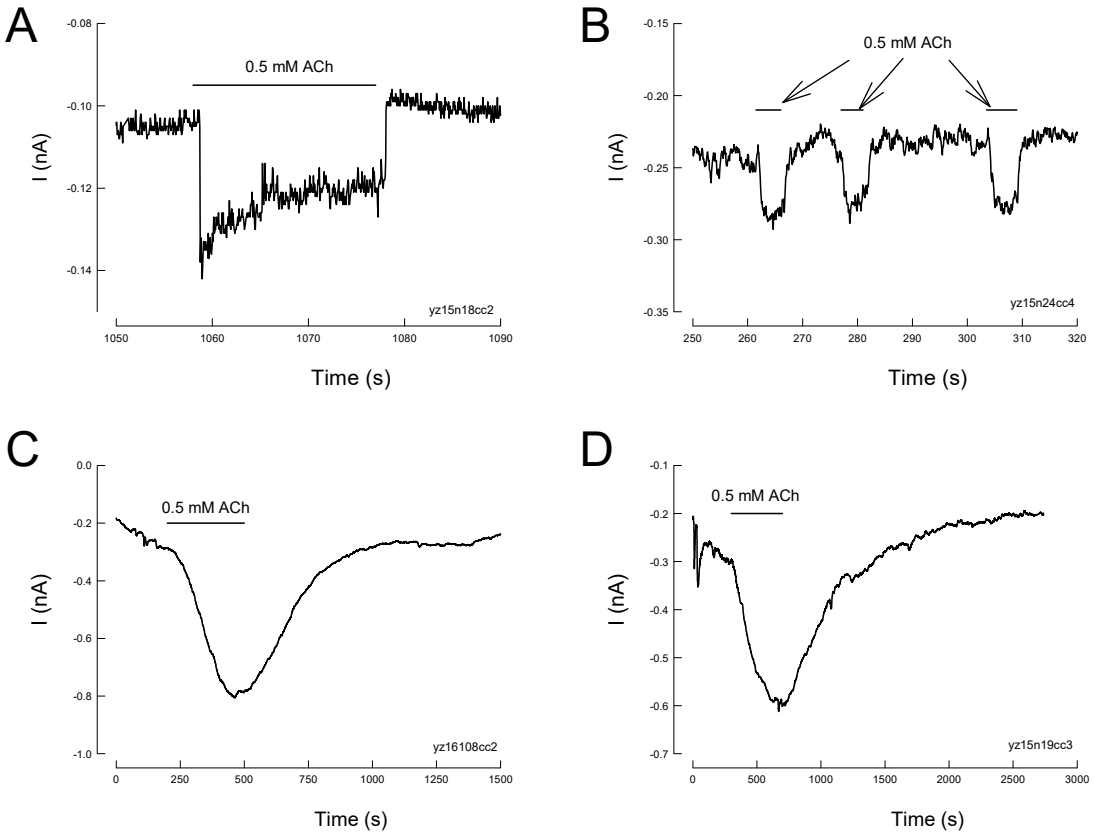

Fig. S1. ACh-evoked inward current in mouse cochlear supporting cells. **A:** ACh-evoked current in single mouse Hensen cell. **B:** The ACh-evoked current is repeatable. The horizonal bars represent the repeated application of ACh in single mouse Deiters cell. **C-D:** ACh-evoked currents in the coupled mouse cochlear supporting cells. Panel C is current recorded from 2-coupled DCs and panel D is current recorded from 3-coupled DCs. Input capacitance in panel C and D was 53.3 and 76.8 pF, respectively.

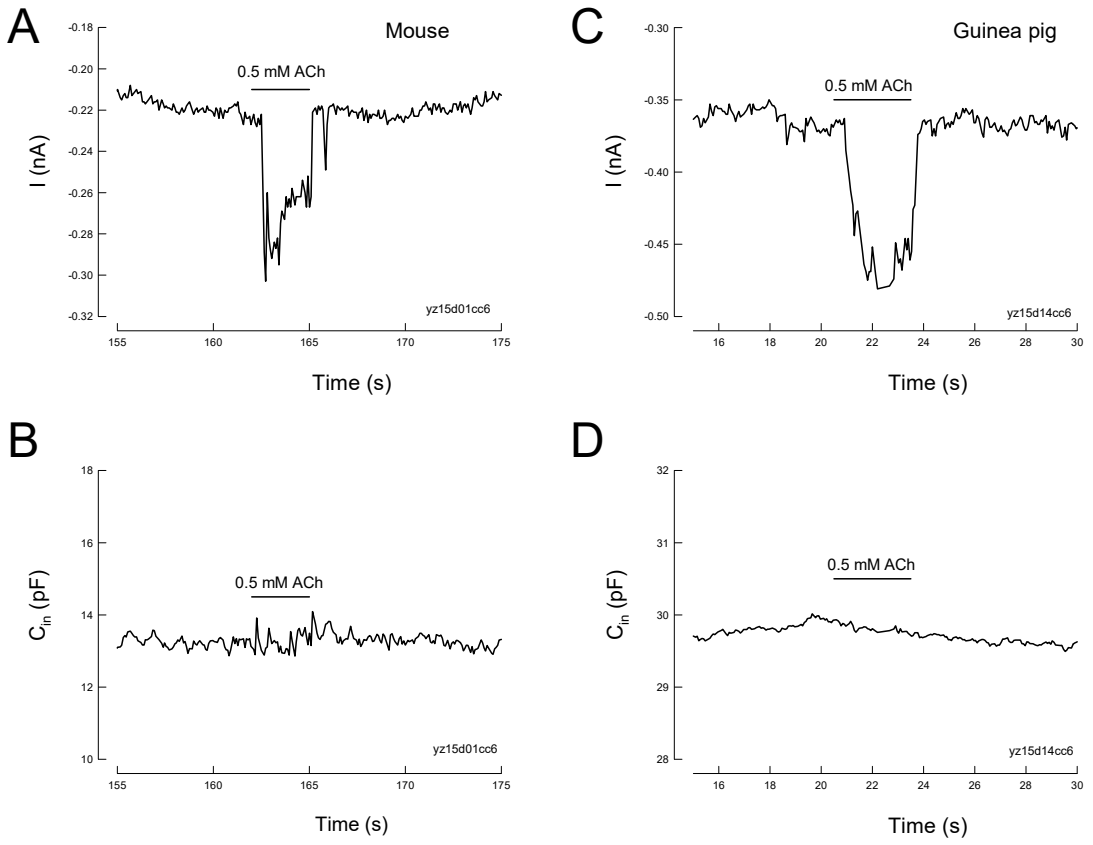

Fig. S2. Input capacitance has no changes in single Deiter cell for ACh application. **A-B:** ACh-induced inward current and measured C_{in} in single mouse Deiters cell. Application of 0.5 mM ACh evoked an apparent inward current in single Deiter cell but did not cause apparent change in C_{in}. **C-D:** ACh-evoked inward current and C_{in} in single Deiters cell in guinea pig. Application of 0.5 mM ACh evoked an apparent inward current but had no apparent change in C_{in}.

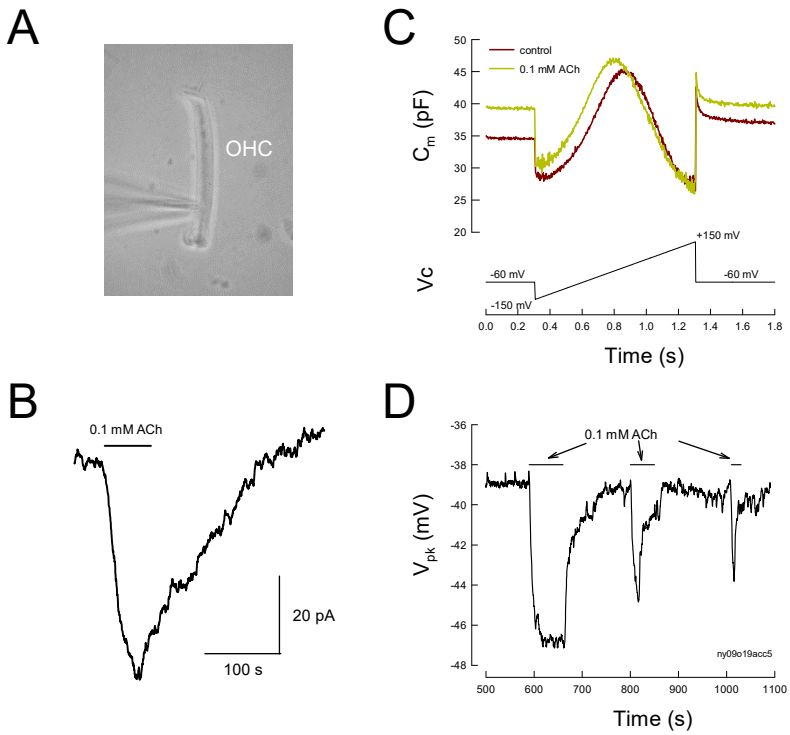

Fig. S3. ACh-evoked inward current in OHC and influence on OHC electromotility in guinea pigs. **A:** A captured image of patch-clamp recording in single OHC. **B:** ACh-evoked inward current in an OHC. A horizontal bar represents application of 0.1 mM ACh. **C:** ACh-induced OHC electromotility associated NLC changes. After application of 0.1 mM ACh, OHC NLC was shifted to left negative voltage side. V_{pk} of NLC was 14.8 and -2.19 mV for control and ACh application, respectively. **D:** ACh-induced OHC electromotility changes is reversible. V_{pk} of NLC was continuously tracked. Application of ACh caused V_{pk} shifted to negative voltage. This shift is reversible and repeatable.

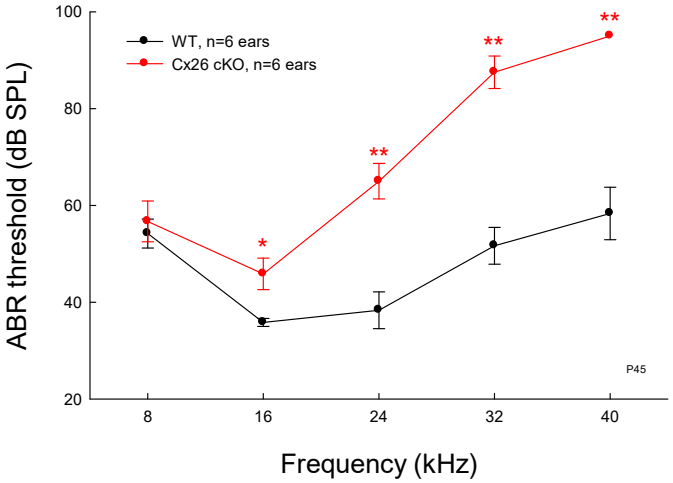

Fig. S4. Reduction of hearing sensitivity in Cx26 cKO mice. Mice were 45 days old. WT littermates serve as control. ABR threshold in Cx26 cKO mice was significantly increased. *: P<0.05, **: P<0.01, two-tail t test.